Journal of Power Sources 249 (2014) 48–58

Contents lists available at ScienceDirect

Journal of Power Sources

journal homepage: www.elsevier.com/locate/jpowsour

Electrochemical anchoring of dual doping polypyrrole on graphene sheets partially exfoliated from graphite foil for high-performance supercapacitor electrode

Yu Song, Jun-Li Xu, Xiao-Xia Liu*

Department of Chemistry, Northeastern University, Wenhua Road, Shenyang 110819, China

HIGHLIGHTS

- Partial exfoliation of graphene is achieved by one-step electrochemical exfoliation.
- Subsequent polypyrrole anchoring was conducted, offering new direction for developing graphene-based materials.
- The obtained Ex-GF/PPy-NDS displays excellent pseudocapacitive properties in the potential window of −0.8 to 0.5 V vs. SCE.

GRAPHICAL ABSTRACT

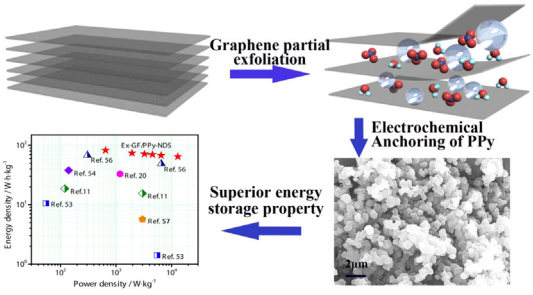

ARTICLE INFO

Article history:
Received 20 August 2013
Received in revised form
27 September 2013
Accepted 23 October 2013
Available online 1 November 2013

Keywords:
Electrochemically partial exfoliation
Graphene
Dual doping polypyrrole
Supercapacitor

ABSTRACT

Partial exfoliation of graphene from graphite foil (GF) is achieved by a convenient one-step electrochemical exfoliation method to afford partially exfoliated graphene electrode (Ex-GF) with graphene sheets standing on GF matrix stably. Electropolymerization of pyrrole is carried out on Ex-GF with 1,5-naphthalene disulfonate (NDS) and 2-naphthalene sulfonate (NMS) as the 'permanent' doping anions to prepare Ex-GF/PPy-NDS and Ex-GF/PPy-NMS, respectively, in which the polymer is anchoring on the surfaces of graphene sheets. The PPy displays an opened structure due to the facilitated homogeneous nucleation on Ex-GF and so exhibits enhanced specific capacitance compared to the polymers deposited on pristine GF (to afford GF/PPy-NDS and GF/PPy-NMS). Specifically, Ex-GF/PPy-NDS film maintains 79% of its specific capacitance when the discharge current density increases from 1 to 20 A g^{-1}. Moreover, discharge potential window of the polymer is enlarged to 1.3 V (from −0.8 to 0.5 V vs. SCE) due to the dual doping mode. Ex-GF/PPy-NDS film displays a high energy density of 82.4 Wh kg^{-1} at the power density of 650 W kg^{-1} and 65.1 Wh kg^{-1} at the power density of 13 kW kg^{-1}. The cyclic charge/discharge stability of the polymer is also improved due to synergistic effect with partially exfoliated graphene.

1. Introduction

Electrochemical capacitors (supercapacitors, SCs) have received increasing attention as a promising energy storage device due to their extremely high power density, reasonable energy density, long cycle life, wide operating temperature range and flexible packaging [1–4]. SCs are superior choice of energy source since they are able to fill up the gap between batteries and conventional electrostatic capacitors. SCs can be used as primary power sources and combine with batteries or fuel cells to construct hybrid charge storage devices as well [4,5].

Graphene, with a 2D structure of sp^2-hybrid carbons, is an ideal candidate for supercapacitor electrode material due to its high conductivity, great mechanical strength, large specific

* Corresponding author. Tel./fax: +86 024 83684323.
E-mail address: xxliu@mail.neu.edu.cn (X.-X. Liu).

0378-7753/$ – see front matter © 2013 Elsevier B.V. All rights reserved.
http://dx.doi.org/10.1016/j.jpowsour.2013.10.102

surface area and perfect porosity effects [3–6]. However, low specific capacitance of carbon-based materials limits their applications, since the charges are mainly accumulated by the primary charge storage mechanism of electrical double-layer (EDLCs) [7]. On the other hand, conducting polymers are widely studied as pseudocapacitive materials because of their high specific capacitance, good electrochemical reversibility, low cost, and facile synthesis processes [8–10]. However, swelling/shrinking of polymer backbones may happen during charge/discharge process and lead to irreversible phase change, which would limit their lifetime and power density [4].

Composites of graphene and conducting polymers are studied to combine the advantages of EDLCs and pseudocapacitive materials [11–23]. These composite materials are usually synthesized by *in situ* chemical polymerization in graphene suspension [12–17], and in most cases a polymer binder (e.g., Nafion and polytetrafluoroethylene) is required as an additive to fabricate electrode from the powder sample. The incorporation of the insulating binder into the electrode would increase the electric resistance of the material and decrease its specific capacitance. Electrochemical polymerization in graphene suspension is a very attractive synthesis method for the composites, since the desired product can be obtained anchoring onto the substrate with appropriate quantity, suitable shape and size in a single step before final application [18–21]. However, connections between graphene sheets in the composites made by both *in situ* chemical and electrochemical polymerization might be blocked by polymeric aggregations, so the effect of graphene on improving electric conductivity for the composites may be weakened [21].

Recently, chemically partial exfoliation of graphene from carbon nanotubes (CNTs) was reported, the obtained partially exfoliated carbon nanotubes displayed an improved capacitance due to the increased effective surface area [24]. Hybrid MnO_2/graphene/CNTs also showed enhanced capacitance because of its 3D architecture with MnO_2 coated on the graphene sheets which were partially exfoliated from CNTs [25]. Other than the benefit from high surface area, the partial exfoliation of graphene also facilitates electronic connections between graphene sheets through the CNT matrix.

Strong oxidizing agents (such as fuming nitric acid/potassium chlorate or sulfuric acid/potassium permanganate) and reducing agents (such as dimethylhydrazine) that are commonly used for chemical exfoliation of graphene by Hummers' method would cause serious pollution problems. This method might also severely damage the honeycomb lattices of graphene [26]. The 'greener' and simpler syntheses of graphene were reported recently which were realized by one-step electrochemical exfoliations [27–32]. Graphene sheets suspending in electrolytes could be obtained with low structure defects through their complete exfoliation from graphite electrodes. Powder samples were obtained after separation from the suspension, so additional procedures are needed to fabricate electrode for further use and in most cases a polymer binder is also required, leading to the increases in electrode resistance. Herein we report electrochemically partial exfoliation of graphene sheets from graphite foil (GF), keeping the electronic connections between graphene sheets through the graphite matrix. The as-synthesized graphene electrode (Ex-GF) could be used directly for its electrochemical property study and subsequent surface modification without any additional procedures.

Polypyrrole (PPy) has obtained great attention in the field of charge storage. It shows good electrochemical performance and pseudocapacitive behaviors in neutral aqueous solutions, and has much lower carcinogenic risks associated with its degradation products compared to polyaniline [10,21]. Through introducing 'permanent' doping anions into the polymer, PPy could store charges in a relatively large potential range due to the 'dual doping' by both anions and cations [33]. In the oxidation process of the dual doped PPy, the cations that doped in the previous reduction process would extract, followed by the insertion of additional anions from the electrolyte. Opposite processes proceed with anion extraction and cation insertion during the reduction of the polymer. The cation-related and anion-related redox of PPy occur in quite a different potential range, leading to an enlarged charge storage potential window for the polymer. Ingram and coworkers reported a dual doped PPy by using polysulfonated aromatic compounds as the permanent doping anions. The polymer displayed an open structure in which the positively charged neighboring polymeric chains were bridged by the polysulfonated aromatic anions. It showed good capacitive behaviors since open channels helped with fast ion transportation and thus allowed the rapid insertion/extraction of cations and anions into/out of the polymer from/to the electrolyte [33].

In this work, electropolymerization of pyrrole is carried out on the partially exfoliated graphene sheets which stand on the GF matrix (Ex-GF). Sulfonated aromatic compounds 1,5-naphthalene disulfonate (NDS) and 2-naphthalene sulfonate (NMS) are used as the 'permanent' doping anions to afford dual doped PPy which anchors on partially exfoliated graphene to fabricate Ex-GF/PPy-NDS and Ex-GF/PPy-NMS electrodes. Homogeneous nucleation of PPy is facilitated on Ex-GF, which enables to build porous microstructure for the polymers and further enhances their specific capacitances. The PPy has a wide potential window of 1.3 V due to the dual doping mode, and shows higher energy density and superior rate capability. Ex-GF/PPy-NDS film demonstrates an energy density of 65.1 Wh kg^{-1} at the power density of 13 kW kg^{-1}, and 82.4 Wh kg^{-1} at the power density of 650 W kg^{-1}. Cyclic charge/discharge stability of the electrode is also improved due to the suppression of graphene re-stacking and PPy expansion/shrinkage.

2. Experimental

2.1. Materials

All the reagents were purchased from Sinopharm Chemical Reagent Co., Ltd. and used as received. Graphite foil (GF) manufactured from natural expanded graphite was obtained from SGL group (Germany).

2.2. Electrochemical partial exfoliation of graphene and subsequent electropolymerization of pyrrole

Electrochemically partial exfoliation of graphene was performed in a three-electrode cell filled with phosphate buffer solution (pH = 6.68) containing 1 M KNO_3, with GF as working electrode, Pt as counter electrode and a saturated calomel electrode (SCE) as reference electrode. Advanced cyclic voltammetric (ACV) scans were carried out on GF for 10 times at 20 mV s^{-1} between −0.5 V and 1.9 V, with a holding at 1.9 V for 6 s in each scan. The obtained partially exfoliated graphene electrode Ex-GF was washed with deionized water to remove any residual solutes.

Partially exfoliated graphene/polypyrrole electrodes, Ex-GF/PPy-NDS and Ex-GF/PPy-NMS, were prepared by electropolymerization of pyrrole on Ex-GF in the solution of 0.2 M pyrrole containing 0.05 M 1,5-naphthalene disulfonic acid and 2-naphthalene sulfonic acid, respectively. The electropolymerization was conducted by cyclic voltammetric scans for 10 times between 0 V and 0.8 V at 50 mV s^{-1}. The obtained electrodes were washed with deionized water and dried for further use. Electropolymerization of pyrrole was also similarly carried out on pristine graphite foil to prepare GF/PPy-NDS and GF/PPy-NMS for comparison. The loading of the polymer was measured by the weight

difference of the electrode (vacuum dried at room temperature) before and after electropolymerization, using Sartorius BT 25 S semi-microbalance with an accuracy of 0.01 mg.

2.3. Characterization

Morphologies of all products were studied by a scanning electron microscope (LEO SUPRA 35, Carl Zeiss, Germany). X-ray photoelectron spectroscopy (XPS) analyses were conducted on an imaging photoelectron spectrometer (Axis Ultra, Kratos Analytical Ltd., UK) with Al K_α radiation as the excitation source. A Fourier transform infrared (FT-IR) spectrophotometer (VERTEX70, Bruker Optics, Germany) was used to obtain vibrational spectra of the materials. Contact angles were measured with a Theta Optical Tensiometer (TL 100, Biolin Scientific, Finland). Raman spectra were obtained on a confocal laser microRaman spectrometer (HR800UV, HoribaJobin Yvon, France) with the excitation wavelength at 633 nm. Electrochemical experiments were performed with a multichannel electrochemical analyzer (VMP3, Bio-Logic-Science Instruments, France). The electrode materials were also analyzed using electrochemical impedance spectroscopy (EIS) in a frequency range of 0.05 Hz–40 kHz, the electrodes were subjected to an applied DC potential of 10 mV during the measurements. All the electrochemical tests were performed in 3 M KCl aqueous solution.

3. Results and discussions

3.1. Electrochemically partial exfoliation of graphene sheets from graphite foil

Oxygen functional groups are helpful for the weakening of van der Waals interactions between graphene layers in graphite and thus facilitate the exfoliation of graphene. If graphite is charged by high voltage (for example 15 V), it would be oxidized too much and fully exfoliated into electrolyte to form graphene suspensions [27,31,32]. In order to control the partial exfoliation of graphene sheets and keep them standing on the graphite matrix stably instead of fully exfoliated into the solution, anodic potential is kept below 1.9 V in this work. Typically, the partial exfoliation is conducted on GF by ACV between −0.5 V and 1.9 V, in which a holding at 1.9 V is conducted for 6 s at each scan. At the moderate positive potential, graphite could be functionalized appropriately to partially overcome the interlayer cohesive energy between graphene sheets. The NO_3^- ions and water molecules could intercalate within graphene sheets, and gas molecules such as O_2 and CO_2 might evolve from water decomposition and carbon oxidation [34], which further help with partial exfoliation of graphene sheets from GF (Fig. 1).

The morphologies of graphite foil (GF) and partially exfoliated graphene on GF (Ex-GF) were investigated by SEM. Fig. 2a–d shows the top view of GF and Ex-GF. It is clear to see that the surface of GF (Fig. 2a and c) is smooth and small graphite flakes are tightly packed on top. After electrochemically partial exfoliation, thin graphene multilayers are formed in small sizes (lateral dimension of one to a few microns with the average thickness of ~7 nm) and stand on top of the Ex-GF electrode (Fig. 2b and d). So the Ex-GF has a preponderance of exposed graphene edge planes on its surface, which will facilitate electron transfer and benefit electrochemical reactions, as the HOMO and LUMO energies are concentrated around the edge of the graphene sheet [6,35]. Side views of GF and Ex-GF are shown in Fig. 2e and f. Ex-GF displays expanded structure and has larger interlayer distance compared to GF, which results from the intercalation of ions and molecules within graphene layers [34,36].

Raman spectroscopy is highly sensitive to electronic structures and is widely used to characterize graphite and graphene materials. The main Raman features of graphitic carbon-based materials are the G and D bands and their overtones. The G band corresponds to the E_{2g} vibrational mode of sp^2-hybrid carbon in graphite, while the D band is associated with vibrations of carbon atoms with dangling bonds in plane terminals of disordered graphite [37]. Therefore, D-peak intensity is often used to characterize graphene sheet disorder and graphene edges [38]. Fig. 3a shows the Raman spectra of pristine graphite foil (GF) and partially exfoliated graphene (Ex-GF). The G band for GF is at 1576 cm^{-1} and D band at 1332 cm^{-1}, which agrees with the typical characters of graphite. After electrochemically partial exfoliation, there is a significant increase in I_D/I_G ratio for Ex-GF compared to GF. This indicates that the electrochemical oxidation and graphene exfoliation lead to partial disorder of graphene layers in the graphite crystal structure as well as a decrease in the size of in-plane sp^2 domains [37,39]. In addition, the wavenumber of G band is 16 cm^{-1} higher for Ex-GF than that for GF. The decreasing of the number of graphene layer and chemical doping may result in up-shift of the G band [36,40]. The reduction of graphene layer number could be furthermore confirmed by 2D band. It is known that the shape, width and position of the 2D peak are very sensitive to the number of graphene layers [41]. For GF, 2D peak is at 2684 cm^{-1} and it could be fitted as two Lorentz peaks. Ex-GF, on the other hand, shows a symmetric 2D peak with a red shift to 2655 cm^{-1}, indicating that few-layer or multi-layer graphene sheets are successfully exfoliated. This is in agreement with SEM results. As the graphene layers are more disordered in Ex-GF, it has a lower I_{2D}/I_G ratio than GF. Similar Raman behaviors were also found in other reported graphene, for example those synthesized by chemical reduction of graphite oxide, step-by-step controllable thermal reduction of graphene oxide, exfoliation of graphitic oxide and conversion from nanodiamond [39,42,43].

XPS is used to study the composition of Ex-GF. Wide region scanning XPS spectra of GF and Ex-GF are shown in Fig. 3b. Main difference is that oxygen and nitrogen peaks are found in the Ex-GF spectrum but not much in GF (Table 1), indicating that oxygen and nitrogen containing groups are introduced during

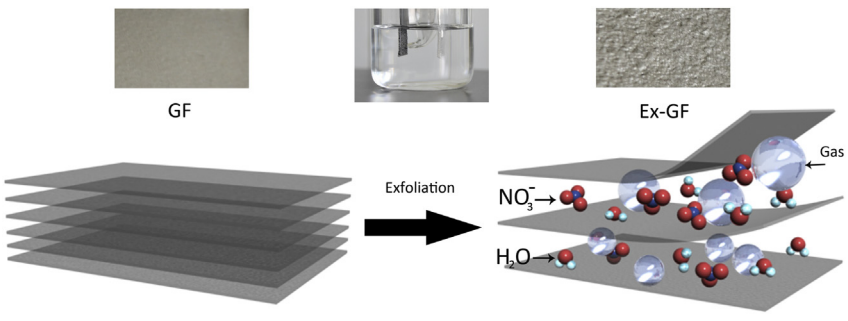

Fig. 1. Graphical mechanism for electrochemically partial exfoliation of graphene sheets from graphite foil.

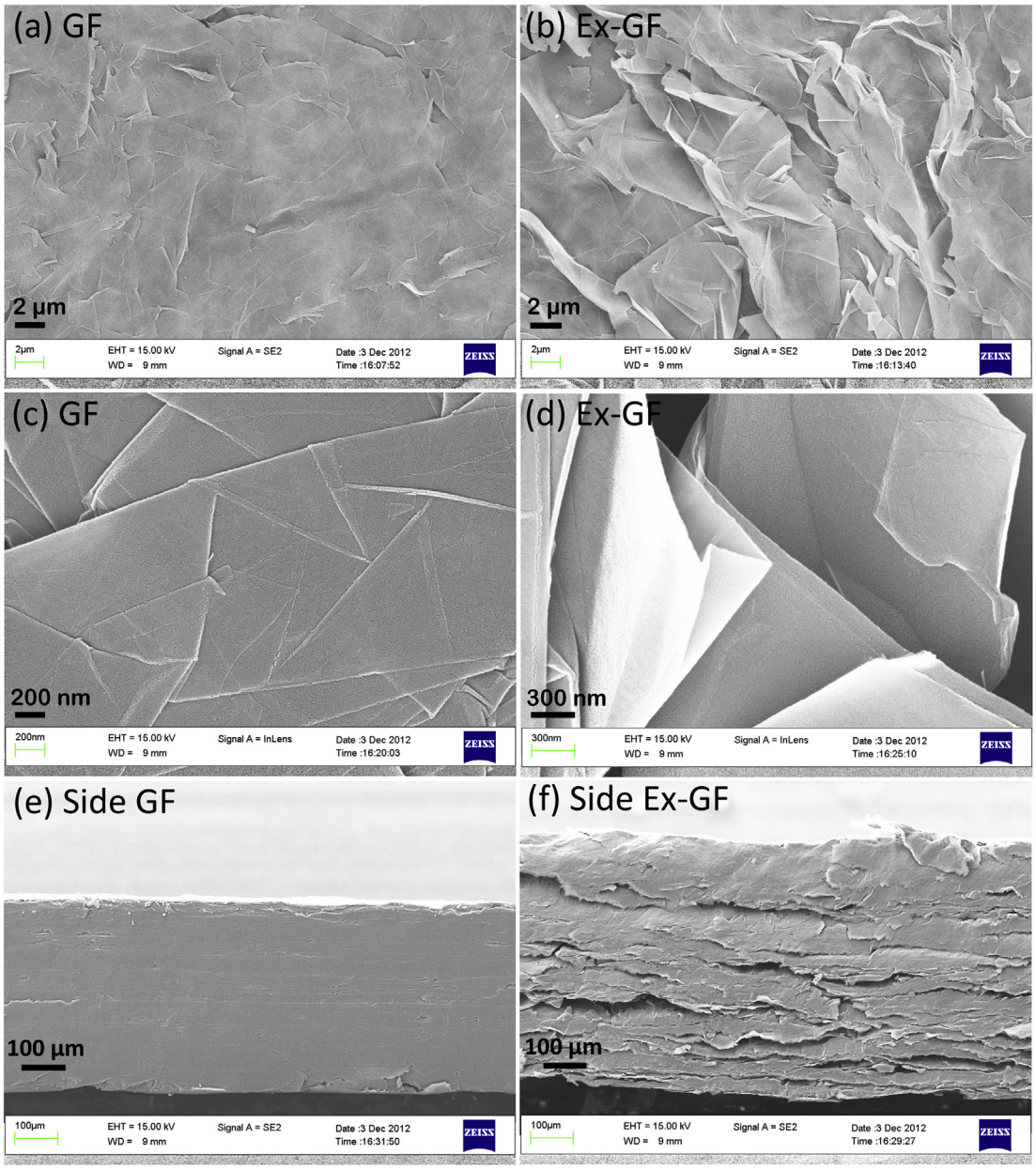

Fig. 2. SEM images of GF (a, c), Ex-GF (b, d) with low (a, b) and high magnification (c, d), together with the side view of GF (e) and Ex-GF (f).

electrochemically partial exfoliation. The C 1s spectrum of Ex-GF is shown in Fig. 3c. It is fitted with four components, which locate at 284.6 eV for C—C, 285.4 eV for C—N, 286.5 eV for C—OH, and 287.7 eV for C═O, respectively [44,45]. The electron-donating functional groups cannot only dramatically improve the wetting behavior of Ex-GF (Fig. S1) but also introduce pseudocapacitive Faradaic reactions [46,47]. Moreover, in the subsequent *in situ* electrochemical polymerization of pyrrole, the functional groups could be used as doping anions which are helpful for the anchoring of the polymer chains on the surfaces of graphene sheets. The π–π interactions between graphene sheets and polymer backbone, as well as the hydrogen bonding between the functional groups of graphene sheets and amino-groups in polymer chains would also play an important role for polymer anchoring [19,48].

GF and Ex-GF electrodes are further studied by cyclic voltammetry in a three-electrode system with 3 M KCl solution as electrolyte. Compared to GF, Ex-GF shows higher current on its cyclic voltammogram (CV), indicating that it has larger surface area than GF (Fig. 3d). In addition, Ex-GF shows a small redox pair, which is caused by its functional groups (Fig. 3d and Fig. S2). The stability of Ex-GF is studied by prolonged cyclic voltammetric scans (Fig. 3d). The CVs keep almost the same up to 1000 cycles, except for the gradual disappearance of the small redox pair after ~300 cycles, which may be due to the partial reduction of the functional groups during the negative scans. These well-overlapped CVs indicate the superior electrochemical stability of Ex-GF in KCl solution. Similar slightly distorted rectangular shapes are also found in the CVs of Ex-GF scanned at various rates up to 200 mV s^{-1} (Fig. S2), suggesting efficient charge accumulation and ion diffusion at the interface between electrode and electrolyte.

3.2. Electrochemical anchoring of dual doping polypyrrole on partially exfoliated graphene sheets

Electropolymerization of pyrrole is conducted on the partially exfoliated graphene electrode Ex-GF by using the sulfonated

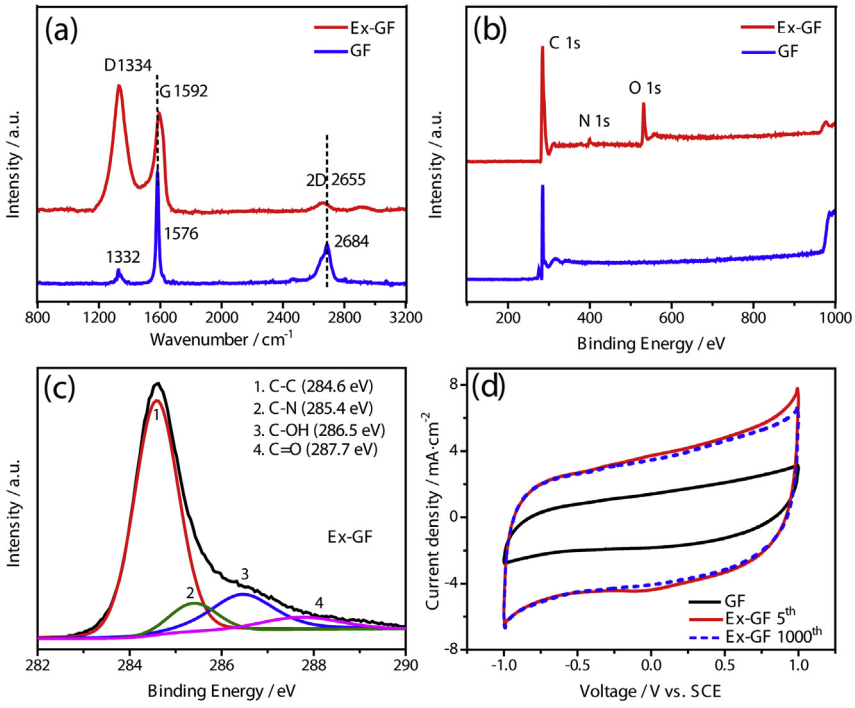

Fig. 3. Raman spectra of Ex-GF and GF (a), wide region scanning XPS spectra of Ex-GF and GF (b), C 1s spectrum of Ex-GF (c), CVs of Ex-GF^{5th}, Ex-GF^{1000th} and GF (d).

compounds, NDS and NMS, as permanent doping anions to afford Ex-GF/PPy-NDS and Ex-GF/PPy-NMS, respectively. For comparison, electropolymerization of pyrrole is also conducted on the pristine GF to make GF/PPy-NDS and GF/PPy-NMS electrodes. The FT-IR spectra of Ex-GF/PPy-NDS and Ex-GF/PPy-NMS are shown in Fig. S3. Typical vibrations of PPy, such as the bands at 1452 and 1560 cm^{-1} (stretching vibrations of pyrrole ring) [49], 1383 and 1272 cm^{-1} (stretching vibrations of sulfonic group and C–N bond, respectively) [17,50], 1122 and 1030 cm^{-1} (doping state of PPy and C–H deformation vibration, respectively) [9,17] are observed. The band at 1633 cm^{-1} is related to the absorbed water molecules [51].

The morphologies of GF/PPy-NDS and GF/PPy-NMS are observed by SEM and shown in Fig. 4a and c. Both of them have the conventional cauliflower-like structure in micron scale sizes. Fig. 4b and d displays the SEM images of Ex-GF/PPy-NDS and Ex-GF/PPy-NMS, respectively. The particle sizes in both cases are smaller than the polymer deposited on GF, and realizing porous open microstructures for the PPy deposited on Ex-GF. During the electrochemically partial exfoliation process, graphene is partially functionalized and thus improves its wetability for better interactions with electrolyte (Fig. S1). It enables the spontaneous nucleation of PPy and facilitates the homogeneous nucleation of the polymer over heterogeneous growth, avoiding the damage of the open polymer structure by the heterogeneous polymerization on the initially-formed PPy particles. The porous microstructure would provide more reactive centers on the polymers to contact with the electrolyte and thus facilitate charge transfer in bulk electrode.

Table 1
Atomic percentage of elements on the surfaces of the electrode materials.

Sample	C [atom%]	O [atom%]	N [atom%]
GF	99.42	0.66	0.00
Ex-GF	88.10	9.66	2.24

The materials are further investigated by XPS. The wide region scanning XPS spectra are in Fig. 4S, while the core level spectra of N 1s peaks are in Fig. 5. The N 1s broad bands could be fitted into three Gaussian peaks with binding energies of 399.8 eV (–NH–), 400.8 eV ($-NH^{+}-$) and 402.2 eV ($=N^{+}-$) [52]. The quinonoid imine (=N–) peak with lower binding energy is usually used to estimate the density of defects in PPy matrix. In this work, this peak is not found for the polymer in any of the four electrodes, indicating that the PPy has few defects [48]. The protonation level of PPy could be calculated from the area percentages of the three fitting peaks. As is shown, the protonation levels of PPy are 41.4% and 32.9% for Ex-GF/PPy-NDS and Ex-GF/PPy-NMS (Fig. 5a and c), respectively, which are much higher than the corresponding polymer deposited on GF (GF/PPy-NDS: 35.4%, Fig. 5b; GF/PPy-NMS: 30.6%, Fig. 5d). It might be caused by additional doping of the polymer by functional groups on the partially exfoliated graphene sheets [19,48]. On the other hand, the PPy doped by NDS shows higher protonation levels (41.4% for Ex-GF/PPy-NDS, Fig. 5a and 35.4% for GF/PPy-NDS, Fig. 5b) than those doped by NMS (32.9% for Ex-GF/PPy-NMS, Fig. 5c and 30.6% for GF/PPy-NMS, Fig. 5d). This difference might be resulted from the higher anionic doping level in NDS-doped polymers than NMS counterparts. The percentage between sulfur in doping anions ([S]) and nitrogen in PPy backbone ([N]) is usually used to estimate the anionic doping level. According to specific peak areas (Table S1), the [S]/[N] percentages are 42.7% and 32.8% for Ex-GF/PPy-NDS and GF/PPy-NDS, respectively, while 40.4% and 27.3% for Ex-GF/PPy-NMS and GF/PPy-NMS, respectively. It indicates that NDS-doped PPy have comparatively higher anionic doping level than NMS counterpart, which is in agreement with the C 1s core level spectra (see below for details). Therefore, higher doping level (both by functional group and through anionic doping) contributes to higher protonation level for Ex-GF/PPy-NDS and thus can give rise to its higher electric conductivity [48].

Fig. 6 shows the C 1s core level spectra of the four electrode materials. The C 1s main peaks are fitted into five Gaussian peaks. The highest binding energy peak at 288.5 eV is assigned to carbonyl

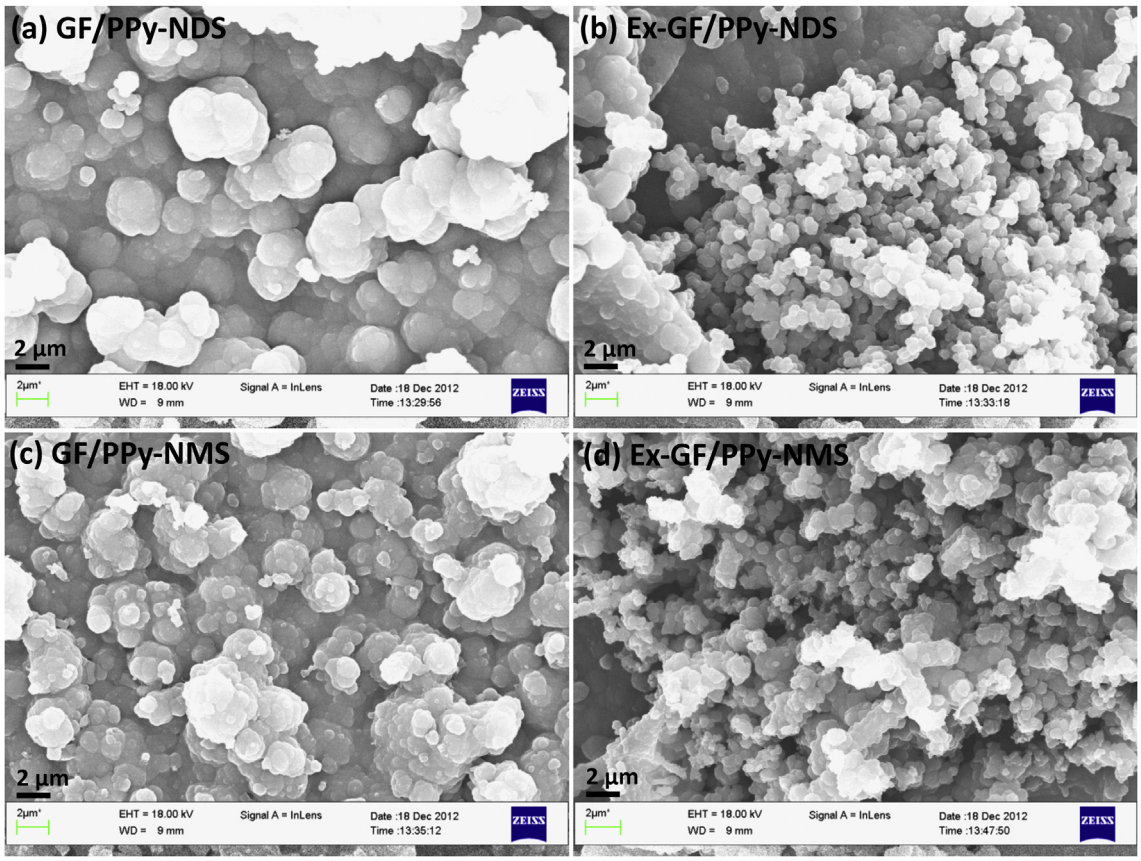

Fig. 4. SEM images of GF/PPy-NDS (a), Ex-GF/PPy-NDS (b), GF/PPy-NMS (c) and Ex-GF/PPy-NMS (d).

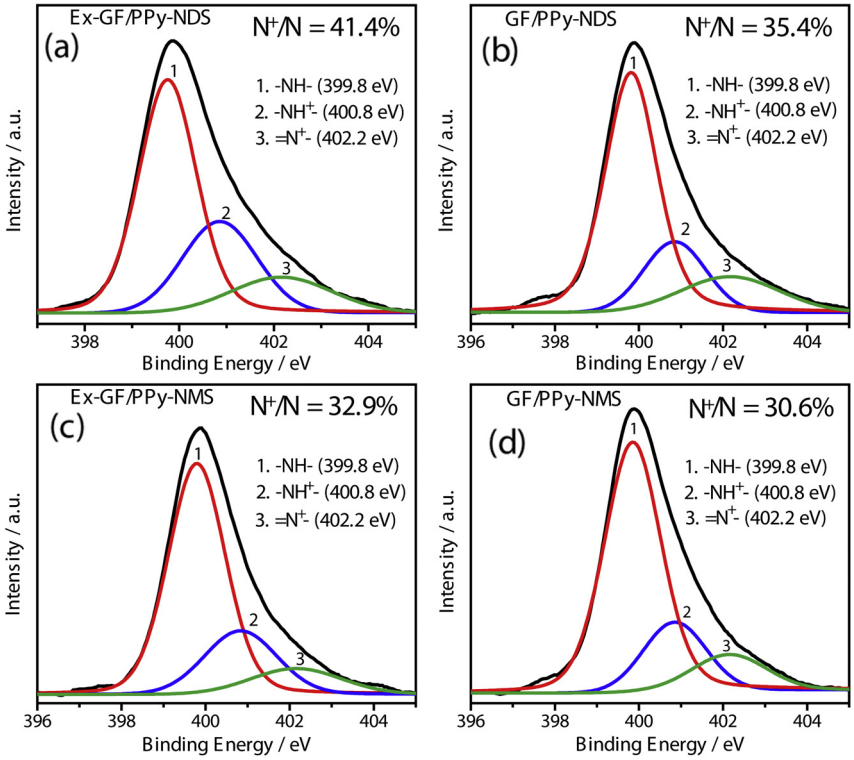

Fig. 5. N 1s XPS core level spectra of Ex-GF/PPy-NDS (a), GF/PPy-NDS (b), Ex-GF/PPy-NMS (c) and GF/PPy-NMS (d).

carbon (C═O), which is formed by the attack of water molecules during polymerization process [53]. The peak with lowest binding energy at 283.7 eV is related to the carbon atoms bonded with sulfur on the doped naphthalene ring, and thus its peak area percentage can be used to estimate the anionic doping level of the polymer [52]. The area percentages of the low binding energy peaks are slightly higher for the polymers in Ex-GF/PPy than for those in GF/PPy (11.1% and 8.0% for Ex-GF/PPy-NDS and Ex-GF/PPy-NMS, respectively, while 9.0% and 6.9% for GF/PPy-NDS and GF/PPy-NMS, respectively), indicating that the formers have higher anionic doping level. It might be related to the open structure of Ex-GF/PPy, which facilitates the contact between electrolyte and the bulk polymers. Moreover, it is also proved by the peak area percentages that the polymers are more anionic doped by NDS than by NMS, contributing to the higher protonation levels of NDS doped polymers (see above). The pyrrole β carbons (C–C) give rise to the peaks at 284.5–284.6 eV, while the peaks of the α carbons (C–N) locate at 285.4–285.5 eV. There is 0.9 eV energy splitting between the α- and β-carbon peaks, which agrees with the reported energy separation in pyrrole monomer [52,54].

The C 1s spectra become asymmetric on the higher binding energy side of the peaks. The asymmetry of the peaks at higher binding energy side is attributed to the 'disorder effect', which corresponds to the Gaussian peak at 286.6–286.7 eV with larger peak width compared to those of the α and β carbons. The 'disorder effect' is related to interchain links and side chains, where the hydrogen atoms originally binding with the β carbons of the pyrrole rings are replaced by carbon atoms as shown in Fig. 7 [52]. From XPS data, the peak area percentages of these disorder type carbons are 24.1% and 19.0%, respectively for Ex-GF/PPy-NDS and GF/PPy-NDS, which are much higher than those for the corresponding polymers of Ex-GF/PPy-NMS and GF/PPy-NMS (16.4% and 13.2%, respectively). It suggests that the interchain interactions are stronger in PPy-NDS than in PPy-NMS [52]. The interchain interactions in NDS doped polymers are further explained in Fig. 7. As is shown, there are two sulfonate groups in opposite positions of the NDS naphthalene ring, and they are likely to dope different PPy chains due to steric hindrance. This would lead to electrostatic cross-linking between adjacent PPy chains, resulting in ordered alignment of polymer chains. Thus, the interchain interactions are facilitated, directing to interchain links and side chains and so showing 'disorder effect' in their C 1s core level XPS spectra [55]. NMS, however, does not behave in the same way, so that NMS-doped PPy do not show such distinct 'disordered effect'. On the other hand, the polymers on Ex-GF have more carbons with the 'disorder effects' than those on GF. The small graphene sheets standing on top of Ex-GF matrix would enhance electron transfer and benefit electrochemical reactions. As a result, the radicals formed during electropolymerization have higher reactivity, leading to higher density of interchain links and side chains distributed within the polymers. Because of this enhanced interchain interactions, 2D conductive networks could be built through the 2D conjugated structure, as demonstrated in Fig. 7. It would improve the electronic conductivity of the polymers, similar to the previously reported PPy doped with PF_6^-, which percolated to metallic regime [52].

3.3. Electrochemical performance of the partially exfoliated graphene/polypyrrole electrodes

Electrochemical activities of the four electrode materials are studied by cyclic voltammetry in 3 M KCl solution at a scan rate of 50 mV s^{-1} (Fig. 8a). The CVs of all the four electrode materials show typical dual doping behaviors with a 'box-like' shape down to −0.8 V. During pyrrole polymerization, the naphthalene sulfonates dope in PPy as 'permanent' dopant, to balance positive charges on the polymer chains. When the polymer is charged by positive scan from its open potential in 3 M KCl, PPy is further oxidized and so additional anions (Cl^-) from the electrolyte insert into the polymer to balance the extra charges (primary doping). In

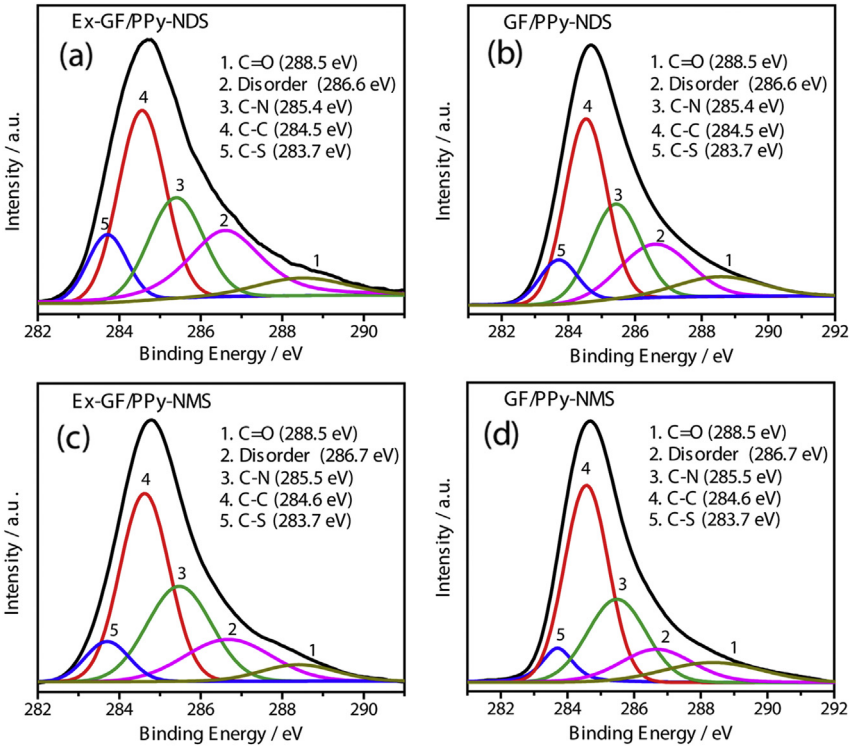

Fig. 6. C 1s XPS core level spectra of Ex-GF/PPy-NDS (a), GF/PPy-NDS (b), Ex-GF/PPy-NMS (c) and GF/PPy-NMS (d).

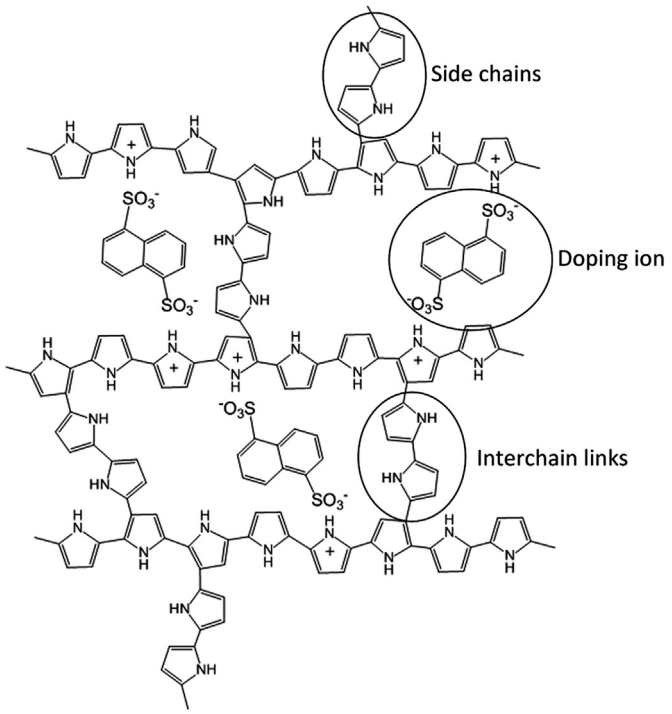

Fig. 7. Schematic chemical structure of PPy doped by NDS.

the negative scan for discharge, the polymer is reduced so the primary doped anions eject from the polymer. However, the 'permanent' doping anions (naphthalene sulfonates) could not eject due to their large sizes. Thus secondary doping by the cations from electrolyte occurs to balance the charges when the polymer is further reduced. The next charging process involves the ejection of cations followed by the insertion of anions from electrolyte [33]. The combination of the primary and secondary doping process results in the 'box-like' shaped CVs. Similar to Naoi and coworkers's work, the reversibility of the cation doping is improved by using 'permanent' doping anions with more sulfonate groups on naphthalene ring [55]. The Ex-GF/PPy electrodes (solid lines) have larger current densities than the corresponding GF/PPy electrodes (dotted lines) as expected. It is due to the increased surface area of Ex-GF-based electrodes and the synergetic effects between Ex-GF and PPy, such as π–π interaction between graphene sheets and polymer backbone, hydrogen bonding between graphene functional groups and polymer amino group, and additional doping by graphene functional groups for the polymer. In order to check the potential window for charge storage, cyclic voltammetric scans are conducted at different potential windows with gradually negative shift of the lower switching potential from 0 V down to −0.8 V. As is shown in Fig. 8b, the CVs of Ex-GF/PPy-NDS approximately follow the same trace on the negative sweeps, suggesting that its stable potential window could be extended down to −0.8 V.

Galvanostatic charge/discharge measurements are performed at a current density of 1 A g^{-1} in 3 M KCl aqueous solution. Typical capacitive behaviors with almost symmetric charge/discharge curves are found for all of the four electrodes (Fig. 8c). The PPy based specific capacitance (C_s) is calculated to be 351, 322, 240 and 148 F g^{-1} for Ex-GF/PPy-NDS, Ex-GF/PPy-NMS, GF/PPy-NDS and GF/PPy-NMS, respectively (calculation details are in Supporting information). The polymers anchoring on Ex-GF have 46% and 118% higher specific capacitance than those on the pristine GF for the NDS and NMS doped PPy, respectively. The specific capacitance of Ex-GF/PPy-NDS film, with a comparatively high loading of the polymer (1.02 mg cm^{-2}) and measured at a relatively high discharge current density (1 A g^{-1}), is also higher than or comparable to the values for recently reported graphene-conducting

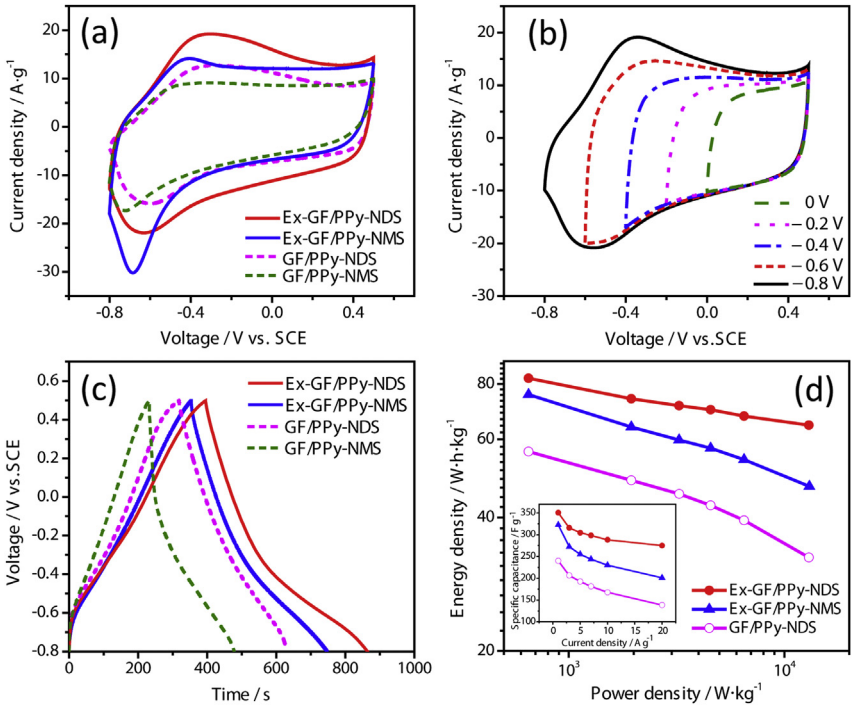

Fig. 8. CVs of Ex-GF/PPy-NDS, Ex-GF/PPy-NMS, GF/PPy-NDS and GF/PPy-NMS in the potential window of −0.8 V to 0.5 V vs. SCE at a scan rate of 50 mV s^{-1} (a); CVs of Ex-GF/PPy-NDS with different lower switching potentials (b); galvanostatic charge/discharge curves of Ex-GF/PPy-NDS, Ex-GF/PPy-NMS, GF/PPy-NDS and GF/PPy-NMS at current density of 1 A g^{-1} (c); Ragone plots of Ex-GF/PPy-NDS, Ex-GF/PPy-NMS and GF/PPy-NDS films, inset shows the specific capacitance of Ex-GF/PPy-NDS, Ex-GF/PPy-NMS and GF/PPy-NDS films at different current densities (d).

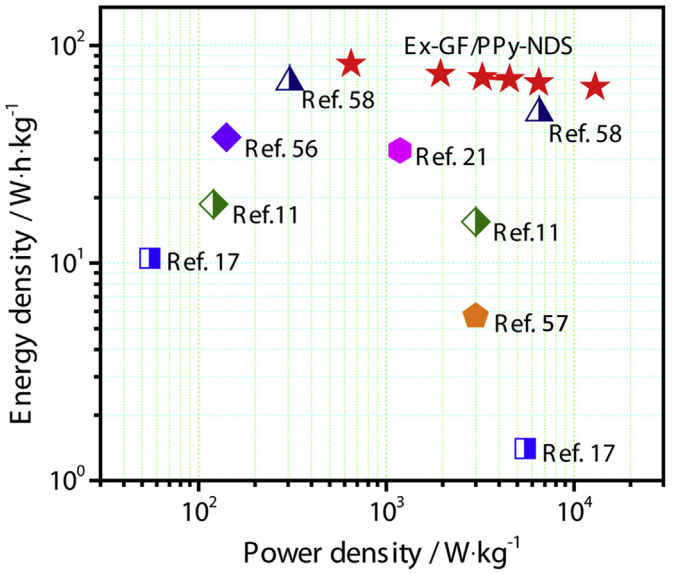

Fig. 9. Ragone plots of the Ex-GF/PPy-NDS film and the values of recently reported graphene-conducting polymer composites for comparison.

polymer composites (Table S2) [11–22]. Significantly, the C_s of Ex-GF/PPy-NDS film remains as high as 275 F g^{-1} even at a much higher discharge current density of 20 A g^{-1} (Fig. 8d inset), which maintains 79% of the C_s at 1 A g^{-1}. It indicates that Ex-GF/PPy-NDS possesses excellent rate capability [11,12,14–20,23]. The specific capacitance of Ex-GF/PPy-NMS and GF/PPy-NDS films decreases to 62% and 58%, respectively, when the discharge current density increases from 1 to 20 A g^{-1}. We are surprised to find that GF/PPy-NMS shows abnormal behaviors in prolonged charge/discharge process as well as cyclic voltammetric scans for 150 cycles (see below for discussions about the cyclic galvanostatic charge/discharge experiments), so we failed to get reliable data for its specific capacitances at different discharge currents. Fig. 8d shows the ragone plots of Ex-GF/PPy-NDS, Ex-GF/PPy-NMS and GF/PPy-NDS films (calculation details are in Supporting information). As is shown, Ex-GF/PPy-NDS film has much higher energy density than the other two when discharged at the same power density. For example, when discharged at a high power density of 13 kW kg^{-1}, Ex-GF/PPy-NDS film demonstrates a high energy density of 64.6 Wh kg^{-1}, which is 37% higher than that of Ex-GF/PPy-NMS and 99% higher than that of GF/PPy-NDS. An extremely high energy density of 82.4 Wh kg^{-1} is derived for Ex-GF/PPy-NDS film when discharged at a power density of 650 W kg^{-1}. Moreover, Ex-GF/PPy-NDS film also shows considerably higher energy density and power density than other recently reported values of graphene-conducting polymer composites which makes it a competitive electrode material for supercapacitors (Fig. 9) [11,17,21,56–58].

The Nyquist plots of the four electrodes displayed in Fig. 10 show distorted semi-circle in the high-frequency region and nearly vertical linear spike in the low frequency region, which is typical for capacitor materials. Their EIS characteristics are listed in Table 2. The charge transfer resistance (R_{ct}) is calculated from the diameter in the real part of distorted semi-circle. The knee frequency f_{knee}, which is the maximum frequency at which predominant capacitive behavior can be maintained, is determined by the crossing of Warburg-type line (inclined 45°) and low-frequency vertical line (Fig. 10). Ex-GF/PPy-NDS has much lower R_{ct} than the other three electrodes. The polymer deposited on the surfaces of the small

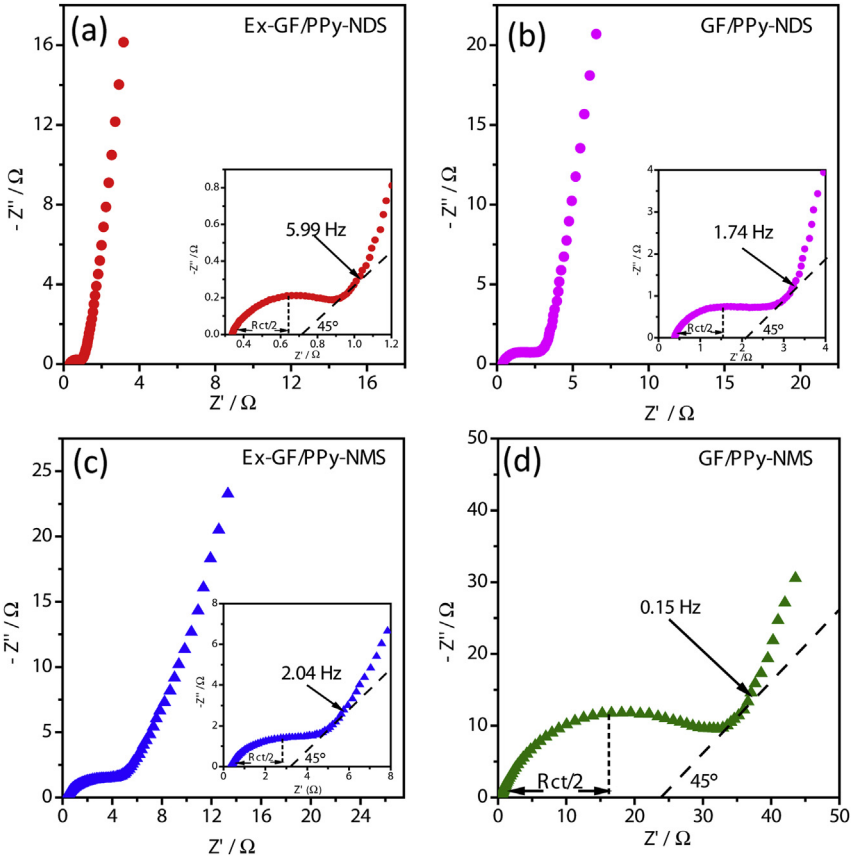

Fig. 10. Nyquist plots of Ex-GF/PPy-NDS (a), GF/PPy-NDS (b), Ex-GF/PPy-NMS (c) and GF/PPy-NMS (d). Insets show the magnified high-frequency regions.

Table 2
EIS characteristics for different electrode materials.

Sample	R_{ct} [Ω]	f_{knee} [Hz]
Ex-GF/PPy-NDS	0.58	5.99
GF/PPy-NDS	2.52	1.74
Ex-GF/PPy-NMS	2.28	2.03
GF/PPy-NMS	35.4	0.15

graphene sheets will benefit fast electron transfer and promote electrochemical reactions [6,35]. Moreover, the open structures of Ex-GF/PPy ensure the easier access of ions for intercalation/deintercalation into/out of the polymer [55]. The enhanced interchain interactions of the polymer in Ex-GF/PPy-NDS also play an important role for decreasing R_{ct}. The Ex-GF/PPy-NDS displays the highest f_{knee}, indicating its fast charging/discharging ability [59].

Cyclic galvanostatic charge/discharge experiments are conducted at 5 A g^{-1} in 3 M KCl aqueous solution for 1000 times on the four electrodes in order to investigate their prolonged charge/discharge behaviors (Fig. 11a). The GF/PPy-NDS film loses 30% of its specific capacitance (from 194 to 137 F g^{-1}) after 1000 cyclings (pink line with circle symbols in Fig. 11a in the web version). Cracks can be seen on the SEM image of GF/PPy-NDS after 1000 cycles (Fig. 11b). It might be caused by repeated doping/de-doping of ions and the related swelling/shrinking of the polymer. On the other hand, the mechanical flexible graphene sheets in Ex-GF/PPy-NDS could provide large elastic buffer space for PPy, which was also found in metal oxide/graphene composites [60]. Thus, no cracking or crumbling is detected on the Ex-GF/PPy-NDS electrode material after 1000 charge/discharge (Fig. 11c). 82% of its specific capacitance (249 of 305 F g^{-1}) is maintained after 1000 cyclings (red line with solid circle symbols in Fig. 11a), indicating that Ex-GF/PPy-NDS is more stable than GF/PPy-NDS. GF/PPy-NMS shows abnormal cyclic charge/discharge behaviors (Fig. 11a, green line with hollow triangle symbols). In the first 400 cycles, the specific capacitance increases along with the cycling. To avoid false verdict from possible errors in experiment, we repeated the experiment for several times and similar abnormal behaviors were observed. Moreover, cyclic voltammetric scans are conducted on GF/PPy-NMS for 150 cycles. The CVs are in Fig. S5 with the inset demonstrating the cathodic current at −0.7 V vs. SCE for different cycles. The CVs of GF/PPy-NMS display similar trends as the cyclic charge/discharge performance. At the first 70 scans, the cathodic current abnormally increases along with the cyclic scans, indicating that the electroactivity increases. This is in agreement with the abnormal increase in specific capacitance. In order to explain this phenomenon, we investigate the morphologies of the 1000-cycled GF/PPy-NMS sample by SEM. Blisters can be seen on surfaces of the cycled GF/PPy-NMS sample (Fig. 11d and the inset for digital photograph). The PPy-NMS film was also electrodeposited on ITO and its self-standing film can be peeled off from the substrate (Fig. 11f), showing that it has good elasticity. So blisters can be formed after swelling of the polymer film during charge/discharge process. We saw that electrolyte spilled out when the blister was punctured by a tweezers, indicating that the electrolyte could also reach the inner surfaces of blisters and so both sides of the blisters could be used for charge storage. As a result, the specific capacitance of GF/PPy-NMS film increases gradually in the first 400 cycles due to the crescent blisters. From the 400th cycle to the 1000th cycle, the specific capacitance decreases 7%. Self-standing PPy-NDS film can also be peeled off from substrate after electrodeposited on ITO, however cracks instead of blisters can be seen on the surfaces of the cycled GF/PPy-NDS sample (Fig. 11b). Only few smaller blisters can be detected on the 1000 charged/discharged sample of Ex-GF/PPy-NMS (Fig. 11e). This may be due to the existence of small graphene sheets standing on Ex-GF matrix, so the electrode substrate has no large enough smooth patch to form intact blisters. After 1000 charge/discharge cycles, Ex-GF/PPy-NMS film loses 9% of its initial capacitance (from 257 to 234 F g^{-1}, blue line with solid triangle symbols). Specifically, the specific capacitance only decreases significantly in the initial 100 cycles and then changes very little in the following 900 cycles (97% is maintained from 242 to 234 F g^{-1}), demonstrating again the improved stability of PPy which anchors on partially exfoliated graphene sheets.

4. Conclusions

Partial exfoliation of graphene was realized by an easy controlled electrochemical process. The large edge to basal plane ratio of small graphene sheets which stand on matrix of graphite foil, facilitates

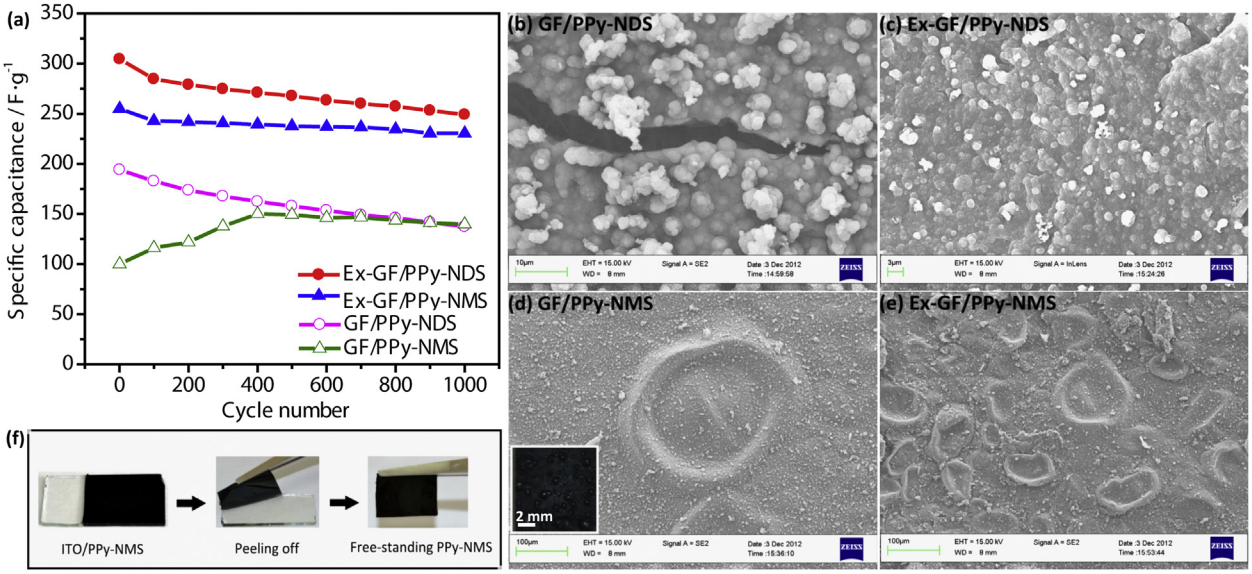

Fig. 11. Cyclic charge/discharge performances of the four electrodes (a), SEM images of the electrodes after galvanostatic charge/discharge for 1000 cycles (b–e), digital photograph for the peeling of free-standing PPy-NMS film (f).

electron transfer and benefits electrochemical reactions. The PPy with open structures was electrochemically anchored on the partially exfoliated graphene to afford Ex-GF/PPy-NDS and Ex-GF/PPy-NMS. In these materials, the electronic connection between graphene sheets can be achieved through the graphite foil matrix, avoiding the blocking of graphene sheets connection by polymeric aggregations. The polymers are anionic and cationic dual doped by using sulfonated aromatic compounds NDS and NMS as the permanent doping anions, leading to large potential window for charge storage. The polymers displayed superior pseudocapacitive properties in a large potential window of 1.3 V from −0.8 V to 0.5 V vs. SCE, enabling their higher energy density. Ex-GF/PPy-NDS film demonstrated an energy density of 65.1 Wh kg^{-1} at the power density of 13 kW kg^{-1}, and of 82.4 Wh kg^{-1} at the power density of 650 W kg^{-1}. Ex-GF/PPy-NDS showed excellent rate capability due to its open structure and the synergistic effects between the two components in the material. 79% of its specific capacitance could be maintained when the discharge current density increased 20 times from 1 to 20 A g^{-1}. The enhanced interchain interactions of the polymer also played an important role for its superior capacitive properties. Intimate contact of the polymer with graphene sheets may be achieved by the doping of PPy with the functional groups in the graphene, and the π−π interaction between aromatic ring of PPy and honeycomb lattices of graphene. This will contribute to the suppressing of the re-stacking of graphene and the volume change of PPy during charge/discharge cycles, leading to improved cyclic charge/discharge stability for the materials. The electrochemically partial exfoliation of graphene and the following pseudocapacitive materials anchoring can offer a new direction for developing new graphene-based materials. In addition, the free standing films of PPy-NMS and PPy-NDS may endow special application for these conducting polymers.

Acknowledgment

Xiao-Xia Liu gratefully acknowledges financial supports from National Natural Science Foundation of China (project number: 21273029) and Research Foundation for Doctoral Program of Higher Education of China (project number: 20120042110024). Jun-Li Xu thanks the financial support from National Natural Science Foundation of China (project number: 51104042).

Appendix A. Supplementary data

Supplementary data related to this article can be found at http://dx.doi.org/10.1016/j.jpowsour.2013.10.102.

References

[1] J.R. Miller, P. Simon, Science 321 (2008) 651–652.
[2] X. Lu, M. Yu, T. Zhai, G. Wang, S. Xie, T. Liu, C. Liang, Y. Tong, Y. Li, Nano Lett. 13 (2013) 2628–2633.
[3] Y. Zhu, S. Murali, M.D. Stoller, K.J. Ganesh, W. Cai, P.J. Ferreira, A. Pirkle, R.M. Wallace, K.A. Cychosz, M. Thommes, D. Su, E.A. Stach, R.S. Ruoff, Science 332 (2011) 1537–1541.
[4] M.D. Stoller, S. Park, Y. Zhu, J. An, R.S. Ruoff, Nano Lett. 8 (2008) 3498–3502.
[5] P. Simon, Y. Gogotsi, Nat. Mater. 7 (2008) 845–854.
[6] J.R. Miller, R.A. Outlaw, B.C. Holloway, Science 329 (2010) 1637–1639.
[7] A.G. Pandolfo, A.F. Hollenkamp, J. Power Sources 157 (2006) 11–27.
[8] L. Yuan, X. Xiao, T. Ding, J. Zhong, X. Zhang, Y. Shen, B. Hu, Y. Huang, J. Zhou, Z.L. Wang, Angew. Chem. Int. Ed. 51 (2012) 4934–4938.
[9] D.P. Dubal, S.H. Lee, J.G. Kim, W.B. Kim, C.D. Lokhande, J. Mater. Chem. 22 (2012) 3044–3052.
[10] L. Yuan, B. Yao, B. Hu, K. Huo, W. Chen, J. Zhou, Energy Environ. Sci. 6 (2013) 470–476.
[11] Q. Wu, Y. Xu, Z. Yao, A. Liu, G. Shi, ACS Nano 4 (2010) 1963–1970.
[12] J. Xu, K. Wang, S.Z. Zu, B.H. Han, Z. Wei, ACS Nano 4 (2010) 5019–5026.
[13] N.A. Kumar, H.J. Choi, Y.R. Shin, D.W. Chang, L. Dai, J.B. Baek, ACS Nano 6 (2012) 1715–1723.
[14] K. Zhang, L.L. Zhang, X.S. Zhao, J. Wu, Chem. Mater. 22 (2010) 1392–1401.
[15] J. Zhang, X.S. Zhao, J. Phys. Chem. C 116 (2012) 5420–5426.
[16] C. Xu, J. Sun, L. Gao, J. Mater. Chem. 21 (2011) 11253–11258.
[17] D. Zhang, X. Zhang, Y. Chen, P. Yu, C. Wang, Y. Ma, J. Power Sources 196 (2011) 5990–5996.
[18] P. Si, S. Ding, X.-W. Lou, D.-H. Kim, RSC Adv. 1 (2011) 1271–1278.
[19] C. Zhu, J. Zhai, D. Wen, S. Dong, J. Mater. Chem. 22 (2012) 6300–6306.
[20] A. Liu, C. Li, H. Bai, G. Shi, J. Phys. Chem. C 114 (2010) 22783–22789.
[21] A. Davies, P. Audette, B. Farrow, F. Hassan, Z. Chen, J.-Y. Choi, A. Yu, J. Phys. Chem. C 115 (2011) 17612–17620.
[22] D.W. Wang, F. Li, J. Zhao, W. Ren, Z.G. Chen, J. Tan, Z.S. Wu, I. Gentle, G.Q. Lu, H.M. Cheng, ACS Nano 3 (2009) 1745–1752.
[23] H.-P. Cong, X.-C. Ren, P. Wang, S.-H. Yu, Energy Environ. Sci. 6 (2013) 1185–1191.
[24] G. Wang, Y. Ling, F. Qian, X. Yang, X.-X. Liu, Y. Li, J. Power Sources 196 (2011) 5209–5214.
[25] Y. Chen, Y. Zhang, D. Geng, R. Li, H. Hong, J. Chen, X. Sun, Carbon 49 (2011) 4434–4442.
[26] C. Gomez-Navarro, R.T. Weitz, A.M. Bittner, M. Scolari, A. Mews, M. Burghard, K. Kern, Nano Lett. 7 (2007) 3499–3503.
[27] C.T.J. Low, F.C. Walsh, M.H. Chakrabarti, M.A. Hashim, M.A. Hussain, Carbon 54 (2013) 1–21.
[28] C.Y. Su, A.Y. Lu, Y. Xu, F.R. Chen, A.N. Khlobystov, L.J. Li, ACS Nano 5 (2011) 2332–2339.
[29] D. Wei, L. Grande, V. Chundi, R. White, C. Bower, P. Andrew, T. Ryhanen, Chem. Commun. 48 (2012) 1239–1241.
[30] J. Wang, K.K. Manga, Q. Bao, K.P. Loh, J. Am. Chem. Soc. 133 (2011) 8888–8891.
[31] J. Lu, J.X. Yang, J. Wang, A. Lim, S. Wang, K.P. Loh, ACS Nano 3 (2009) 2367–2375.
[32] N. Liu, F. Luo, H. Wu, Y. Liu, C. Zhang, J. Chen, Adv. Funct. Mater. 18 (2008) 1518–1525.
[33] M.D. Ingram, H. Staesche, K.S. Ryder, J. Power Sources 129 (2004) 107–112.
[34] J.C.B. Charles, A. Goss, Eugene A. Irene, Royce W. Murray, Anal. Chem. 65 (1993) 1378–1389.
[35] D.A.C. Brownson, L.J. Munro, D.K. Kampouris, C.E. Banks, RSC Adv. 1 (2011) 978–988.
[36] P.R. Singh, X. Zeng, J. Phys. Chem. C 115 (2011) 17429–17439.
[37] J. Shen, Y. Hu, M. Shi, X. Lu, C. Qin, C. Li, M. Ye, Chem. Mater. 21 (2009) 3514–3520.
[38] D. Deng, X. Pan, L. Yu, Y. Cui, Y. Jiang, J. Qi, W.-X. Li, Q. Fu, X. Ma, Q. Xue, G. Sun, X. Bao, Chem. Mater. 23 (2011) 1188–1193.
[39] G. Wang, J. Yang, J. Park, X. Gou, B. Wang, H. Liu, J. Yao, J. Phys. Chem. C 112 (2008) 8192–8195.
[40] G. Eda, M. Chhowalla, Adv. Mater. 22 (2010) 2392–2415.
[41] A.C. Ferrari, J.C. Meyer, V. Scardaci, C. Casiraghi, M. Lazzeri, F. Mauri, S. Piscanec, D. Jiang, K.S. Novoselov, S. Roth, A.K. Geim, Phys. Rev. Lett. 97 (2006) 187401–187404.
[42] I. Jung, D.A. Dikin, R.D. Piner, R.S. Ruoff, Nano Lett. 8 (2008) 4283–4287.
[43] K.S. Subrahmanyam, S.R.C. Vivekchand, A. Govindaraj, C.N.R. Rao, J. Mater. Chem. 18 (2008) 1517–1523.
[44] P.L. Chiu, D.D. Mastrogiovanni, D. Wei, C. Louis, M. Jeong, G. Yu, P. Saad, C.R. Flach, R. Mendelsohn, E. Garfunkel, H. He, J. Am. Chem. Soc. 134 (2012) 5850–5856.
[45] E. Bekyarova, M.E. Itkis, P. Ramesh, C. Berger, M. Sprinkle, W.A. de Heer, R.C. Haddon, J. Am. Chem. Soc. 131 (2009) 1336–1337.
[46] S.L. Candelaria, B.B. Garcia, D. Liu, G. Cao, J. Mater. Chem. 22 (2012) 9884–9889.
[47] L. Sun, L. Wang, C. Tian, T. Tan, Y. Xie, K. Shi, M. Li, H. Fu, RSC Adv. 2 (2012) 4498–4506.
[48] J. Wang, Y. Xu, J. Zhu, P. Ren, J. Power Sources 208 (2012) 138–143.
[49] H.D. Tran, K. Shin, W.G. Hong, J.M. D'Arcy, R.W. Kojima, B.H. Weiller, R.B. Kaner, Macromol. Rapid Commun. 28 (2007) 2289–2293.
[50] Y. Wang, Z. Iqbal, S. Mitra, J. Am. Chem. Soc. 128 (2006) 95–99.
[51] L. Cammarata, S.G. Kazarian, P.A. Salter, T. Welton, Phys. Chem. Chem. Phys. 3 (2001) 5192–5200.
[52] J. Joo, J.K. Lee, S.Y. Lee, K.S. Jang, E.J. Oh, A.J. Epstein, Macromolecules 33 (2000) 5131–5136.
[53] C.-C. Hu, X.-X. Lin, J. Electrochem. Soc. 149 (2002) A1049–A1057.
[54] L. Atanasoska, K. Naoi, W.H. Smyrl, Chem. Mater. 4 (1992) 988–994.
[55] S. Suematsu, Y. Oura, H. Tsujimoto, H. Kanno, K. Naoi, Electrochim. Acta 45 (2000) 3813–3821.
[56] H. Wang, Q. Hao, X. Yang, L. Lu, X. Wang, Nanoscale 2 (2010) 2164–2170.
[57] P.A. Mini, A. Balakrishnan, S.V. Nair, K.R. Subramanian, Chem. Commun. 47 (2011) 5753–5755.
[58] Q. Hao, H. Wang, X. Yang, L. Lu, X. Wang, Nano Res. 4 (2010) 323–333.
[59] M. Hughes, G.Z. Chen, M.S.P. Shaffer, D.J. Fray, A.H. Windle, Chem. Mater. 14 (2002) 1610–1613.
[60] Z.-S. Wu, G. Zhou, L.-C. Yin, W. Ren, F. Li, H.-M. Cheng, Nano Energy 1 (2012) 107–131.